

2-6-2024

Sulfate Enhances the Adsorption and Retention of Cu(II) and Zn(II) to Dispersed and Aggregated Iron Oxyhydroxide Nanoparticles

Emma M. Kocik
University of Pennsylvania


Abigail Kim
University of Pennsylvania

Miranda L. Aiken
Chapman University, maiken@chapman.edu

Lauren Smith
Chapman University

Christopher S. Kim
Chapman University, cskim@chapman.edu

Follow this and additional works at: https://digitalcommons.chapman.edu/sees_articles

 Part of the [Environmental Chemistry Commons](#), [Oceanography Commons](#), and the [Other Oceanography and Atmospheric Sciences and Meteorology Commons](#)

Recommended Citation

Kocik, E.M., Kim, A., Aiken, M.L., Smith, L., Kim, C.S., 2024. Sulfate enhances the adsorption and retention of Cu(II) and Zn(II) to dispersed and aggregated iron oxyhydroxide nanoparticles. *Appl. Geochem.* 162, 105929. <https://doi.org/10.1016/j.apgeochem.2024.105929>

This Article is brought to you for free and open access by the Science and Technology Faculty Articles and Research at Chapman University Digital Commons. It has been accepted for inclusion in Biology, Chemistry, and Environmental Sciences Faculty Articles and Research by an authorized administrator of Chapman University Digital Commons. For more information, please contact laughtin@chapman.edu.

Sulfate Enhances the Adsorption and Retention of Cu(II) and Zn(II) to Dispersed and Aggregated Iron Oxyhydroxide Nanoparticles

Comments

This article was originally published in *Applied Geochemistry*, volume 162, in 2024. <https://doi.org/10.1016/j.apgeochem.2024.105929>

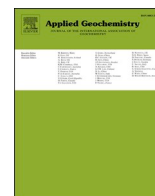
Creative Commons License



This work is licensed under a [Creative Commons Attribution 4.0 License](https://creativecommons.org/licenses/by/4.0/).

Copyright

The authors



Sulfate enhances the adsorption and retention of Cu(II) and Zn(II) to dispersed and aggregated iron oxyhydroxide nanoparticles

Emma M. Kocik^{a,b}, Abigail Kim^b, Miranda L. Aiken^b, Lauren Smith^b, Christopher S. Kim^{b,*}

^a Department of Earth and Environmental Sciences, University of Pennsylvania, Philadelphia, PA, USA

^b Schmid College of Science & Technology, Chapman University, Orange, CA, USA

ARTICLE INFO

Editorial handling by Yuanzhi Tang

Keywords:

Iron oxyhydroxides
Copper
Zinc
Sulfate
EXAFS
nanoparticles

ABSTRACT

The adsorption and retention of metal ions to nanoscale iron (hydr)oxides in aqueous systems is significantly influenced by prevailing environmental conditions. We examined the influence of sulfate, the second most common anion in seawater that is present in many other natural aquatic systems, on the adsorption and retention of Cu(II) and Zn(II) to synthetic iron oxyhydroxide nanoparticles (NPs) and their aggregates. Batch uptake experiments with monodisperse NPs and NPs aggregated by changes in pH, ionic strength, and temperature were conducted over sulfate concentrations ranging from 0 to 0.30 M. The introduction of 0.03 M sulfate significantly increased the initial adsorption and retention of Zn(II) and Cu(II) compared to sulfate-free conditions; with increasing sulfate >0.03 M, Zn(II) retention continuously increased, while Cu(II) retention was considerably more variable but increased slightly. NP aggregation, when induced by pH and ionic strength, was positively correlated with metal ion retention, while aggregation temperature was negatively correlated with both adsorption and retention. Aqueous geochemical modeling indicated that Zn(II) readily complexes with sulfate to form ZnSO₄ (aq), but that stable aqueous CuSO₄ species are uncommon. EXAFS spectroscopic analysis suggests structural incorporation of Zn(II) and Zn(II)-sulfate ternary surface complexation, while Cu(II) primarily forms inner-sphere bidentate surface complexes. Collectively, the effects of sulfate in both reducing surface charge repulsion, initiating ternary surface complexation, and enabling structural incorporation aid to enhance both metal adsorption and retention to iron oxyhydroxide NPs and their aggregates.

1. Introduction

Metal contamination poses a significant threat to human health and the environment. Elevated exposure to metals can result from anthropogenic activities such as mining, industrial production, and unregulated effluent release (Guo and S. Barnard, 2013; Van Der Merwe et al., 2011). Highly enriched concentrations of metals are particularly prevalent in abandoned mine wastes at metal ore mining sites (Luo et al., 2020; Rytuba, 2000), where the release and attenuation of metals including copper, zinc, iron, mercury, and lead involves complex geochemical reactions at the solid-water interface and can impact the health of humans and the surrounding ecosystem (Balali-Mood et al., 2021).

In aquatic systems, the fate of dissolved metal contaminants is often controlled by their sorption to mineral surfaces. When sorbed to mineral surfaces, the metal is less bioaccessible and, therefore, less toxic (García-Sánchez et al., 1999; Hochella, 1990). However, changes in aqueous

geochemical conditions, particularly pH, can release or desorb metals from mineral surfaces, thus increasing their potential bioaccessibility and toxicity (Singh et al., 2008). Although numerous studies have been conducted on metal ion sorption and retention at the bulk mineral-water interface (Shi et al., 2021), significantly fewer studies have examined metal desorption at the mineral-water interface (Auffan et al., 2009).

Naturally occurring iron oxyhydroxide nanoparticles (FeOOH NPs) such as goethite (α -FeOOH) and ferrihydrite play an important role in the geochemical cycling of trace metals and metalloids (Blowes et al., 2005; Waychunas et al., 2002). Due to their high surface area and wide variation in chemical and physical properties, nanoparticles behave and react differently from their macroscale counterparts (Gilbert et al., 2009; Guo and S. Barnard, 2013; Waychunas et al., 2002). Under many natural geochemical conditions, FeOOH NPs aggregate rapidly based on environmental factors such as ionic strength, pH, and temperature (Banfield et al., 2000; Dale et al., 2015; Stegemeier et al., 2015; Yuwono et al., 2012). For example, an increase in ionic strength decreases the electrical

* Corresponding author.

E-mail address: cskim@chapman.edu (C.S. Kim).

<https://doi.org/10.1016/j.apgeochem.2024.105929>

Received 12 November 2023; Received in revised form 18 January 2024; Accepted 26 January 2024

Available online 6 February 2024

0883-2927/© 2024 The Authors. Published by Elsevier Ltd. This is an open access article under the CC BY license (<http://creativecommons.org/licenses/by/4.0/>).

double-layer thickness required to offset the particles' surface charge, inducing aggregation (Brown Jr and Parks, 2001; Hou et al., 2007; Li and Xu, 2008). Increases in solution pH towards the point of zero charge (pH of 7.0–9.0 for FeOOHs) lower the surface charge density of the particles (Dzombak and Morel, 1991), resulting in reduced interparticle electrostatic repulsions and allowing particles to aggregate (Gilbert et al., 2007; Lowry et al., 2004; Stumm and Morgan, 2012). Further, increasing solution temperature accelerates the thermal motion of the particles, causing an increase in collisions and thus aggregation events (Gilbert et al., 2009).

The presence of anions such as chloride has also been demonstrated to impact metal ion sorption and retention to nanoparticles and their aggregates. For example, at relatively low chloride concentrations (0.1 M), Zn(II) retention to FeOOH NPs is reduced; however, retention is increased at concentrations closer to that of seawater (0.6 M). This was concluded to result from the formation of aqueous Zn–Cl ternary surface complexes and reduction in weaker outer-sphere zinc sorption complexes (Chesne and Kim, 2014).

Sulfate is another common anion found in natural freshwaters (0.00003–0.0003 M, (EPA, 2003), seawater (~0.03 M, EPA 2003), and acid mine drainage sites (as high as 2.0 M (Nordstrom and Alpers, 1999)). Several investigators have observed that the presence of sulfate can enhance metal sorption to goethite (Ali and Dzombak, 1996; Collins et al., 1999; Elzinga et al., 2001; Liu et al., 2018; Ostergren et al., 2000; Webster et al., 1998; Zhang and Peak, 2007), which has been attributed to an alteration of electrostatic charge at the iron oxide surface (Balistreri and Murray, 1982; Collins et al., 1999), precipitation of metal-sulfate salt on the mineral surface (Weesner and Bleam, 1998), and formation of ternary surface complexes sorbed to iron oxide substrates (Ali and Dzombak, 1996; Ostergren et al., 2000). The phenomenon of substrate aggregation, in addition to the presence of sulfate, may introduce further complexities to the mechanisms of metal ion adsorption and retention to FeOOH NP mineral surfaces.

The purpose of this study is to investigate the impact of sulfate across a wide range of concentrations on Zn(II) and Cu(II) adsorption and retention to both unaggregated and aggregated FeOOH NPs through macroscopic adsorption/desorption batch experiments, extended X-ray absorption fine edge structure (EXAFS) spectroscopy, and geochemical modeling. Macroscopic batch uptake experiments can characterize the effects of both sulfate concentration and FeOOH NP aggregation on metal uptake and the strength of the metal binding to the mineral surface. EXAFS analysis allows detailed structural analysis to identify the modes of metal ion uptake and retention, and geochemical modeling under the macroscopic experimental conditions will identify the proportions of aqueous metal species present under these conditions. We hypothesize that the effect of sulfate will be similar to that of chloride, where increasing sulfate concentration will result in both enhanced metal adsorption and retention. We also predict that highly aggregated FeOOH NPs will have lower adsorption rates due to less available surface area, but greater retention due to the entrapment of metal ions in interstitial space.

2. Methods

2.1. Iron oxyhydroxide nanoparticle synthesis and aggregation

Iron oxyhydroxide nanoparticles (FeOOH NPs) were synthesized by a flash microwave technique (Guyodo et al., 2003). A solution of 0.25 M sodium bicarbonate was filtered through a 0.20 μm Nylon filter and added dropwise to an equal volume of 0.20 M ferric nitrate. The mixture was capped in an HDPE bottle and shaken on a rotator table for 3 h, venting the solutions to remove generated CO_2 at 30-min intervals. The solution was then heated in a conventional microwave in 30 s intervals, with 2–3 s of manual stirring between intervals until the solution boiled (~2.5 min), initiating the formation of FeOOH NPs. The suspension was immediately submerged in an ice bath for rapid cooling to halt the

growth of the nanoparticles, then washed in deionized (DI) water within 1000 MWCO dialysis tubing for 5 days (≥ 3 water replacements/day) until pH and conductivity had stabilized. The resulting monodisperse NPs are 5–10 nm in diameter with a solids concentration of 6.4 ± 0.2 g/L, surface area of 305 ± 13 m^2/g , and identified as 6-line ferrihydrite with a small proportion of goethite or goethite-like features based on our prior characterization by DLS, BET surface area analysis, and XRD (Chesne and Kim, 2014; Dale et al., 2015; Kim et al., 2008; Stegemeier et al., 2015).

FeOOH NP aggregation was induced by changes in pH, ionic strength, or temperature following established procedures (Chesne and Kim, 2014; Dale et al., 2015; Stegemeier et al., 2015). Monodisperse NPs were transferred to 1000 MWCO dialysis tubing lengths and placed into solutions at pH 5.0, 8.0 or 10 and NaNO_3 concentrations of 0.1 M or 1.0 M (Table 1). Solutions were replaced once daily for 5 days. Following aggregation, the tubes were transferred to a control solution (0.001 M NaNO_3 , pH 5.0) that was changed 2 times per day for 5 days until the pH equilibrated at ~4.5. To aggregate the NP suspensions under elevated temperatures, aliquots were placed into ovens in tightly capped HDPE bottles at 25 °C, 50 °C, or 75 °C (Table 1) for 4 days. Dynamic light scattering from our previous studies confirmed an increase in average NP diameter due to aggregation by elevated pH, ionic strength, and temperature (Chesne and Kim, 2014), and that NP aggregates maintained their relative aggregation state following re-equilibration in control conditions and did not return to their original dispersed structure (Dale et al., 2015).

2.2. Macroscopic batch uptake experiments

Macroscopic Zn(II) and Cu(II) adsorption and desorption experiments were conducted with the unaggregated FeOOH NPs as well as each FeOOH NP aggregate. To initiate metal ion adsorption, 5 mM Zn (NO_3)₂ or Cu(NO_3)₂ and 0.1 M NaNO_3 solutions were added to the NP suspensions to achieve a metal concentration of 0.5 mM, ionic strength of 0.001 M, and solids concentration of 0.17 g/L (Chesne and Kim, 2014). The pH of the suspension was then adjusted upwards to 6.50 ± 0.05 for Cu(II) samples and 7.50 ± 0.05 for Zn(II) samples using 100 μL aliquots of 0.1 M NaOH to optimize metal uptake based on previous experiments and calculations (Dzombak and Morel, 1991). The resulting suspension was sealed in an HDPE bottle and placed on a shaker table at 90 rpm for 18 ± 1 h to enable metal ion adsorption.

Following adsorption, three 40 mL aliquots were set aside for analysis as a control (0 M sulfate) condition in triplicate. The remaining suspension was separated into additional 40 mL aliquots, and appropriate volumes of a 1.8 M Na_2SO_4 stock solution were added to achieve sulfate concentrations ranging from 0 to 0.18 M for all nanoparticle suspensions. For the unaggregated NPs, additional experiments were conducted at 0.24 and 0.3 M sulfate to correlate with EXAFS experimental conditions (see next section). The suspensions were agitated on a shaker table at 90 rpm for 18 ± 1 h, then split into two 20 mL aliquots, with one referred to as the “adsorbed” sample and set aside. The other “retained” sample was produced by reducing the solution pH to 5.00 ± 0.05 using 20 μL aliquots of 0.1 M HNO_3 and placing the suspension on

Table 1

Nanoparticle aggregation conditions. Condition altered to induce aggregation is indicated in bold in each row.

Aggregation condition	NaNO_3 concentration	pH	Temperature
Control	0.001 M	5.0	RT (~20 °C)
pH 8.0	0.001 M	8.0	RT (~20 °C)
pH 10.0	0.001 M	10.0	RT (~20 °C)
0.1 M	0.1 M	5.0	RT (~20 °C)
1.0 M	1.0 M	5.0	RT (~20 °C)
25 °C	0.001 M	5.0	25 °C
50 °C	0.001 M	5.0	50 °C
75 °C	0.001 M	5.0	75 °C

the shaker for another 2.0 ± 0.5 h to enable metal ion desorption from the NP surfaces.

All samples were centrifuged at 3000 rpm for 15 min, with supernatants decanted and filtered through a $0.20 \mu\text{m}$ Nylon syringe filter. The pH of the filtrate was further reduced to ≤ 2.0 using $20 \mu\text{L}$ aliquots of ultrapure 70% HNO_3 for dissolved Cu and Zn analysis with an Agilent 5110 SVDV inductively coupled plasma optical emission spectrometer (ICP-OES). ICP-OES results were used to calculate metal ion adsorption and retention to the substrates following each experimental step. All experiments were conducted in triplicate, with macroscopic data averaged and standard errors calculated.

2.3. Extended X-ray absorption fine structure (EXAFS) spectroscopic analysis

EXAFS spectroscopy of selected unaggregated NP samples over a sulfate concentration range of 0–0.3 M was performed at beamline 11-2 at the Stanford Synchrotron Radiation Lightsources (SSRL). Zn K-edge (9659 eV) and Cu K-edge (8979 eV) spectra were collected in fluorescence mode on damp pastes mounted on Teflon sample holders sealed with 1.5 mm Kapton tape using a 100-element high-throughput germanium detector. Aluminum filters were used to reduce Fe K-edge fluorescence, while Cu and Zn metal foils were used as monochromator energy calibration standards.

Spectra were analyzed using SIXPack software package version 1.4 (Webb, 2005). Each scan was deadtime-corrected to account for signal loss from the saturation of detector channels and then averaged. The averages were then converted into k -space with k^3 -weighting and Fourier transformed. Fits were performed using the shell-by-shell fitting method, with single-shell scattering paths generated in SIXPack using Feff6l (Kim et al., 2008) over k -ranges of 3.0 – 11.5 \AA^{-1} for zinc and 3.0 – 9.5 \AA^{-1} for copper.

2.4. Geochemical modeling

Speciation diagrams were created using the Geochemist's Workbench (GWB) software (Bethke et al., 2023) using the thermodynamic equilibrium database thermo.dat values for Zn and Cu aqueous species. The fraction of each stable aqueous species was calculated as a function of sulfate concentration using the relevant thermodynamic equilibrium equations and beta values, determining the concentration of each species by factoring the solubility product of sodium sulfate into the equilibrium. Aqueous Zn and Cu concentrations were calculated using the experimental results from macroscopic adsorption control experiments (see Table 1). The initial fluid composition for the geochemical model was established using the lab experimental conditions of 0.5 mM Zn (II)/Cu(II), 8.26 mg/L O_2 (aq), and pH 5.0, with 1.8 M NaSO_4 titrated into solution to the desired sulfate concentration.

3. Results

3.1. Zn(II) adsorption and retention to iron oxyhydroxide nanoparticles in the presence of sulfate

3.1.1. Macroscopic adsorption/desorption

Across both control (unaggregated) and aggregated NPs, the adsorption (at pH 7.0) and desorption (at pH 5.0) behaviors of Zn(II) as a function of sulfate concentration are broadly similar (Fig. 1). Specifically, the initial extent of Zn(II) adsorption upon introduction of sulfate at 0.03 M is significantly enhanced relative to sulfate-free conditions, increasing from an average of $77 \pm 10\%$ to $86 \pm 7\%$ Zn adsorption across control and aggregated NPs. Subsequent increases of sulfate up to 0.30 M yield either no or relatively minimal additional Zn(II) adsorption, resulting in a visible “stepwise” increase in Zn(II) adsorption upon the initial introduction of 0.03 M sulfate.

After the pH-induced desorption step to pH 5.0, a similar increase in

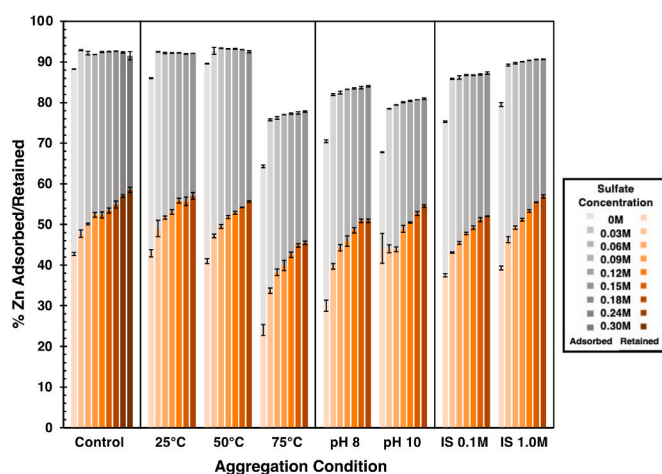


Fig. 1. Percentages of Zn(II) adsorbed (gray) and retained (orange) to unaggregated control FeOOH nanoparticles and nanoparticles aggregated by temperature, pH, and ionic strength (IS) over varying sulfate concentrations. Error bars represent standard errors of triplicate measurements.

Zn(II) retention to the NPs upon the introduction of sulfate is also visible, increasing from an average of $38 \pm 7\%$ to $43 \pm 5\%$. In contrast with the adsorption behavior, however, Zn(II) retention continues to increase significantly with sulfate concentration, following a generally logarithmic growth curve up to 0.18 M sulfate (average $53 \pm 4\%$). In the case of the control NPs, Zn(II) retention is additionally enhanced at the highest sulfate concentrations of 0.24 M (57%) and 0.30 M (58%).

Effects of NP aggregation mechanism on adsorption/desorption behavior and extent are apparent although subtle. Compared to the control sample, NPs aggregated at $25 \text{ }^\circ\text{C}$ and $50 \text{ }^\circ\text{C}$ as well as those aggregated in a 1.0 M ionic strength solution displayed comparable initial adsorption and retention behavior. The other NP aggregates displayed lower Zn(II) adsorption across the sulfate concentration range examined, with the sample aggregated at $75 \text{ }^\circ\text{C}$ yielding the lowest adsorption level of all NP aggregates. The extent of Zn(II) retention to the NP aggregates, however, was generally comparable to that of the control NPs across the sulfate concentrations examined, with only the $75 \text{ }^\circ\text{C}$ -aggregated NPs presenting consistently lower levels of Zn(II) retention. Aggregates produced at higher pH (10.0) and ionic strength (1.0 M) showed greater Zn(II) retention than aggregates produced at lower pH (8.0) and ionic strength (0.1 M).

3.1.2. Spectroscopic analysis

Zn K-edge EXAFS spectra collected on control (unaggregated) NPs exhibit only minor visual differences between the spectra of the “adsorbed” and “retained” samples under sulfate-free conditions, evidenced primarily in the increase of second-neighbor features in the Fourier transforms (Fig. 2). With increasing sulfate concentration, however, distinct features in both the EXAFS spectra (particularly at $\sim 5.5 \text{ \AA}^{-1}$ and $\sim 7.5 \text{ \AA}^{-1}$) and the Fourier transforms of the retained samples are readily apparent, displaying most prominently at sulfate concentrations ranging from 0.09 to 0.18 M. These features then diminish, but are still visible, at the highest sulfate concentrations (0.24–0.30 M).

Quantitative shell-by-shell fitting of the EXAFS spectra (Table 2) reveals relatively constant first-neighbor Zn–O coordination numbers and distances (average 4.0 ± 0.1 and $1.98 \pm 0.004 \text{ \AA}$, respectively) in the retained samples across all sulfate concentrations examined, signifying tetrahedral coordination of Zn(II) in the sorbed state to the FeOOH NPs. In contrast, the two Zn–Fe shells at separate interatomic distances ($3.33 \pm 0.02 \text{ \AA}$ and $3.49 \pm 0.02 \text{ \AA}$) exhibit significant changes in coordination number that correspond with the visual changes in the spectra,

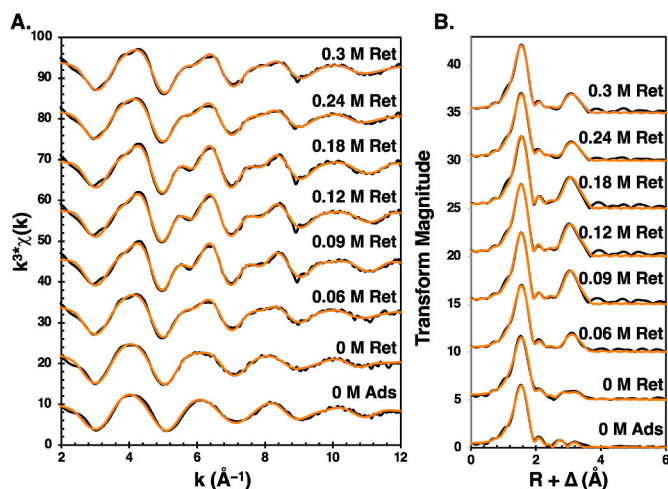


Fig. 2. Fitted zinc K-edge EXAFS spectra (A) and Fourier transformations (B) for adsorbed (Ads) and retained (Ret) unaggregated FeOOH nanoparticle samples at various sulfate concentrations. Black lines = data, orange = fits.

increasing in value from the “adsorbed” to “retained” states and increasing further in the retained state as sulfate concentration increases to 0.18 M, then diminishing but remaining elevated compared to the control spectrum at 0.24 M and 0.30 M. Of the two Zn–Fe shells, the shell at the shorter interatomic distance exhibits a greater absolute and relative increase in coordination number (from 1.1 to 3.9, a 255% increase) than the shell at longer interatomic distance (from 1.4 to 2.7, a 93% increase). The interatomic distances of both Zn–Fe shells also lengthen from the “adsorbed” to “retained” state and as sulfate concentration increases up to 0.09 M, then decline with progressively higher sulfate concentrations. Attempts to fit the second-neighbor features using Zn–S single-shell scattering interactions yielded poorer fits than those using Zn–Fe interactions and therefore were not considered in the final fitting analysis.

The shorter (~3.3 Å) and longer (~3.5 Å) fitted Zn–Fe distances have been observed in prior studies by our group and others, and are interpreted to represent bidentate corner-sharing sorption complexes of Zn (II) sorbed to goethite (Dale et al., 2015; Juillot et al., 2008; Kim et al., 2008; Stegemeier et al., 2015; Waychunas et al., 2002) and ferrihydrite (Juillot et al., 2008; Lee and Anderson, 2005; Nachttegaal and Sparks, 2004; Trivedi et al., 2001), respectively. Previous mineralogical analysis of FeOOH NPs synthesized via the same method were identified as primarily 6-line ferrihydrite with some goethite characteristics (Chesne and Kim, 2014), consistent with the current spectroscopic analysis. The lengthening of Zn–Fe interatomic distances has also been observed in our earlier studies and interpreted as a shift upon desorption towards Zn retention to sites with a lower degree of surface disorder, indicating that such sites are more stable than their relaxed surface site counterparts

Table 2

Zinc EXAFS spectroscopic fitting results. Second shell Debye-Waller values were fixed at 0.01 \AA^2 . ΔCN = percent change in coordination number compared to sulfate-free (0 M sulfate) retained sample.

Sulfate Concentration	Sorption Step	Zn–O		Zn–Fe 1		Zn–Fe 2		E_0 shift	R factor				
		CN	ΔCN	R (\AA^{-1})	$\sigma^2(\text{\AA}^2)$	CN	ΔCN			R (\AA^{-1})	ΔCN	R (\AA^{-1})	
0M	Adsorbed	3.7(1)	–	1.98(1)	0.0079	0.8(3)	–	3.18(2)	0.9(3)	–	3.41(2)	3.9(6)	0.0074
0M	Retained	4.4(1)	–	1.99(1)	0.0099	1.1(3)	–	3.27(2)	1.4(4)	–	3.45(2)	4.5(6)	0.0080
0.06M	Retained	4.3(1)	–2%	1.99(1)	0.0086	1.7(4)	55%	3.34(2)	1.9(5)	36%	3.49(3)	4.5(6)	0.0076
0.09M	Retained	3.8(2)	–14%	1.97(1)	0.0067	3.9(7)	255%	3.39(2)	2.2(7)	57%	3.54(3)	4.4(7)	0.0103
0.12M	Retained	3.8(3)	–14%	1.97(1)	0.0066	3.9(6)	255%	3.38(2)	2.7(6)	93%	3.53(2)	4.3(7)	0.0086
0.18M	Retained	3.7(2)	–16%	1.97(1)	0.0063	3.6(7)	227%	3.38(2)	2.7(7)	93%	3.52(3)	4.6(8)	0.0116
0.24M	Retained	4.2(2)	–5%	1.99(1)	0.0084	1.8(5)	64%	3.34(2)	2.0(5)	43%	3.49(3)	4.3(7)	0.0071
0.30M	Retained	4.2(1)	–5%	1.99(1)	0.0083	1.9(5)	73%	3.34(3)	2.1(5)	50%	3.49(2)	4.5(6)	0.0081

(Dale et al., 2015; Juillot et al., 2008; Kim et al., 2008; Stegemeier et al., 2015; Waychunas et al., 2002).

3.2. Cu(II) adsorption and retention to iron oxyhydroxide nanoparticles in the presence of sulfate

3.2.1. Macroscopic adsorption and desorption

The macroscopic adsorption and desorption behavior of Cu(II) on control and aggregated NPs in the presence of sulfate is considerably more variable than that of Zn(II) (Fig. 3). The same stepwise increase in metal ion adsorption can generally be observed upon the initial introduction of sulfate at 0.03 M (increase from an average of $75 \pm 7\%$ to $92 \pm 5\%$); however, the extent of Cu(II) adsorption with increasing sulfate concentration above 0.03 M is generally constant but in some cases declines (pH 10 aggregate) or continues to increase (0.1 M ionic strength aggregate).

After the pH-induced desorption step, a modest increase in Cu(II) retention upon the introduction of sulfate is observed across both the control and aggregated NPs (from an average of $22 \pm 13\%$ to $32 \pm 10\%$). With progressively higher sulfate concentrations, Cu(II) retention tends to increase but with much more variability than observed with Zn (II). As with the Zn(II) sorption results, the 75 °C aggregate features the lowest adsorption of Cu(II) and among the lowest Cu(II) retention across the experimental sulfate concentration range.

3.2.2. Spectroscopic analysis

Copper K-edge EXAFS spectra show relatively subtle changes between the adsorbed and retained Cu at various sulfate concentrations

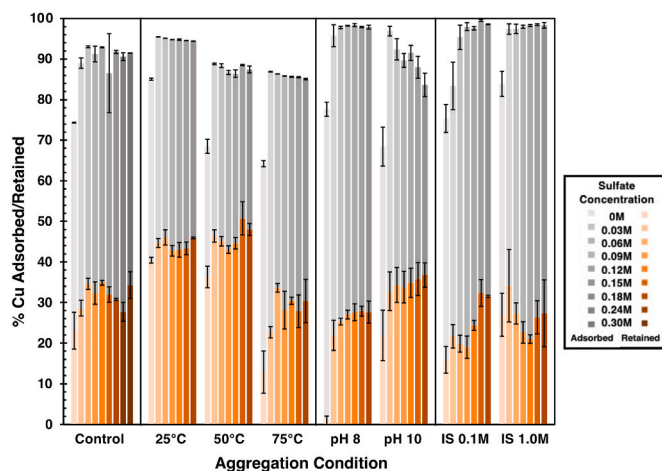


Fig. 3. Percentages of Cu(II) adsorbed (gray) and retained (orange) to unaggregated control FeOOH nanoparticles and nanoparticles aggregated by temperature, pH, and ionic strength (IS) over varying sulfate concentrations. Error bars represent standard errors of triplicate measurements.

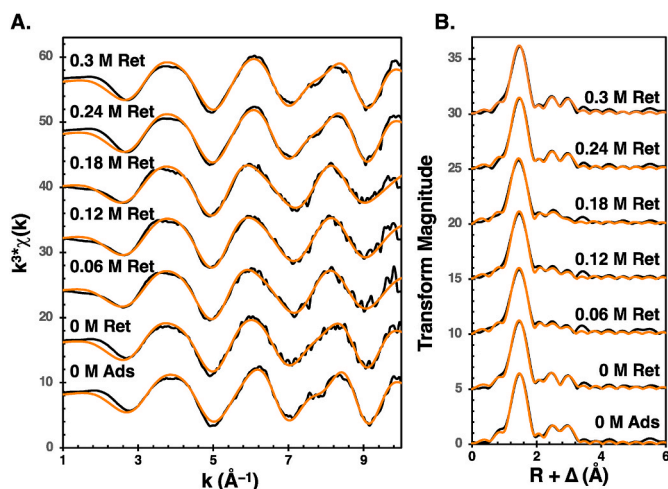


Fig. 4. Fitted copper K-edge EXAFS spectra (A) and Fourier transformations (B) for adsorbed (Ads) and retained (Ret) unaggregated FeOOH nanoparticle samples at various sulfate concentrations. Black lines = data, orange = fits.

(Fig. 4). A shoulder feature in the EXAFS spectra at $k = 7.5 \text{ \AA}^{-1}$, which is most prominent at the lowest (0 M) and highest (0.24 M, 0.30 M) sulfate concentrations and is less visible in the EXAFS spectra collected at intermediate (0.06–0.18 M) sulfate concentrations, corresponds with more prominent second-neighbor features in the Fourier transforms. Shell-by-shell fitting of the spectra (Table 3) shows that the first-shell neighbor is unchanging across all adsorbed.

and retained samples and is best fit by a Cu–O scattering interaction with CN of 3.3 ± 0.3 , indicating a primarily tetrahedral coordination environment. The average Cu–O interatomic distance of $1.95 \pm 0.01 \text{ \AA}$ is consistent with the equatorial bonds in a Jahn-Teller distorted Cu(II) complex and other studies investigating Cu sorption onto iron oxides (Bochatay et al., 1997; Ponthieu et al., 2006). Fits to the second-neighbor features were initially attempted with Cu–S scattering interactions but resulted in poor fits relative to Cu–Fe interactions. Accordingly, the second-neighbor features were best fit as Fe atoms at interatomic distances of $3.08 \pm 0.01 \text{ \AA}$ and $3.31 \pm 0.01 \text{ \AA}$, which correspond to inner-sphere bidentate edge-sharing sorption complexes (Parkman et al., 1999) and bidentate corner-sharing sorption complexes (Alcacio et al., 2001; Peacock and Sherman, 2004), respectively.

Changes in Cu–Fe coordination numbers support the visual interpretation of the EXAFS spectra, with Cu–Fe coordination numbers (CNs) diminishing at intermediate sulfate concentrations of 0.06–0.18 M (–27% and –52% average declines at the shorter and longer interatomic distances, respectively) relative to the higher coordination numbers at the lowest (0 M), then recovering at the highest (0.18 M, 0.24 M) sulfate concentrations (+12% and –5% at the shorter and longer interatomic distances, respectively). These CN changes are also correlated with Cu–Fe interatomic distances, which lengthen slightly at the intermediate sulfate concentrations and may again represent preferential ion

retention at sorption sites with lower surface disorder.

3.3. Geochemical modeling

Geochemical modeling of Zn species abundance within the experimental parameters indicates that the dominant species of Zn in the absence of sulfate is $\text{Zn}_{(\text{aq})}^{2+}$. Upon introduction of sulfate into the system, the proportion of $\text{ZnSO}_4_{(\text{aq})}$ increases logarithmically, becoming the dominant species of zinc at 0.025 M SO_4^{2-} . ZnSO_4 continues to increase in proportion with sulfate concentration up to 0.30 M, but at a slower rate (Fig. 5). Similarly, in the absence of sulfate, dissolved copper is present dominantly as $\text{Cu}_{(\text{aq})}^{2+}$ with a minor fraction present as $\text{CuOH}_{(\text{aq})}^+$. Following the addition of sulfate, the $\text{CuSO}_4_{(\text{aq})}$ species appears and increases logarithmically; however, it represents no more than ~0.005% of total Cu over the experimental range, with copper speciation remaining predominantly as Cu^{2+} and CuOH^+ across all examined sulfate concentrations.

4. Discussion

4.1. Effect of sulfate on Zn(II) and Cu(II) sorption and retention

The initial introduction of sulfate into the binary metal ion-nanoparticle aqueous systems significantly increased both Zn(II) and Cu(II) ion adsorption and retention across a wide range of NP aggregates. Prior studies similarly documented an increase in divalent metal ion uptake (e.g. Cd, Cu, Hg, Mg, Pb, Zn) in the presence of sulfate, attributing the enhanced uptake to a combination of electrostatic surface charge reduction through sulfate inner- and outer-sphere adsorption at the mineral surface and the formation of ternary metal-sulfate surface sorption complexes (Hoins et al., 1993; Juang and Wu, 2002; Kim et al., 2004; Ostergren et al., 2000; Swedlund et al., 2009). However, most of these studies examined the effect of sulfate at considerably lower concentrations ($\leq 0.003 \text{ M}$) more closely approximating those of natural freshwater systems, while sulfate concentrations in the present study (0.03–0.3 M) range from seawater concentrations to those observed in brines and acid mine drainage.

Under these more elevated sulfate conditions, the primary mechanisms of increased metal ion uptake appear to vary and are dependent on metal ion behavior and sulfate concentration. Geochemical modeling indicates that at sulfate concentrations greater than 0.025 M, Zn is dominant in the aqueous phase as $\text{ZnSO}_4_{(\text{aq})}$. This suggests that the initial stepwise increase in Zn(II) adsorption and retention at 0.03 M sulfate is likely due to adsorption of the neutral $\text{ZnSO}_4_{(\text{aq})}$ species, thus forming Type A-style ternary surface complexes similar to those concluded by Ostergren et al. (2000). The inability to fit Zn–S scattering interactions in the EXAFS analysis is likely due to the low atomic number of sulfur and the long interatomic distance between Zn and S in such a ternary surface complex.

As sulfate concentration increases up to 0.18 M, spectroscopic analysis of the unaggregated control retained samples shows a significant increase in Zn–Fe coordination numbers compared with sulfate-free

Table 3

Copper EXAFS spectroscopic fitting results. Second shell Debye-Waller values were fixed at 0.01 \AA^2 . ΔCN = percent change in coordination number compared to sulfate-free (0 M sulfate) retained sample.

Sulfate Concentration	Sorption Step	Cu–O				Cu–Fe 1			Cu–Fe 2			E_0 shift	R factor
		CN	ΔCN	R (\AA^{-1})	$\sigma^2(\text{\AA}^2)$	CN	ΔCN	R (\AA^{-1})	CN	ΔCN	R (\AA^{-1})		
0M	Adsorbed	3.1(1)	–	1.95(7)	0.00278	1.6(4)	–	3.04(1)	2.1(5)	–	3.32(2)	–9.3	0.0076
0M	Retained	3.3(1)	–	1.95(1)	0.00361	1.7(4)	–	3.05(1)	2.0(5)	–	3.29(2)	–10.6	0.0067
0.06M	Retained	3.2(2)	–3%	1.95(1)	0.00353	1.1(5)	–35%	3.12(4)	0.9(6)	–55%	3.31(6)	–10.8	0.0129
0.12M	Retained	3.2(5)	–3%	1.95(1)	0.00333	1.2(6)	–29%	3.12(5)	1.1(7)	–45%	3.32(6)	–10.2	0.0140
0.18M	Retained	3.4(5)	3%	1.95(1)	0.00413	1.4(6)	–18%	3.12(4)	0.9(7)	–55%	3.33(7)	–11.7	0.0130
0.24M	Retained	3.2(3)	–3%	1.95(1)	0.00296	1.6(4)	12%	3.05(2)	1.9(5)	–5%	3.31(2)	–9.9	0.0064
0.30M	Retained	3.3(4)	0%	1.95(1)	0.00363	1.7(5)	12%	3.04(2)	1.9(6)	–5%	3.30(2)	–9.6	0.0109

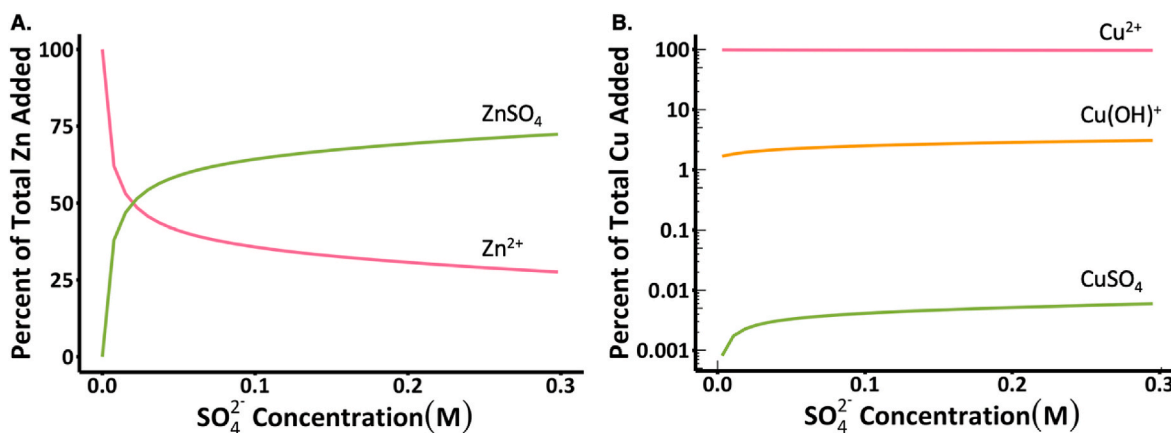


Fig. 5. Aqueous geochemical models of zinc (A) and copper (B) speciation over experimental sulfate concentrations (0–0.30 M). Modeling was conducted under experimental conditions of 0.5 mM Zn(II) or Cu(II), 8.26 mg/L O₂ (aq), and pH 5.0.

conditions. These larger coordination numbers indicate Zn structural incorporation and/or substitution into the Fe-hydroxide structure, suggesting that sulfate in this concentration range facilitates Zn incorporation into the surface, possibly through surface charge neutralization. At even higher sulfate concentrations (up to 0.30 M), however, the Zn–Fe coordination numbers decline to values between those of the sulfate-free conditions and the more intermediate sulfate concentrations examined; this implies that at the highest sulfate concentrations examined less structural incorporation is taking place, possibly through surface site saturation or multilayer formation of sulfate ions.

The behaviors and modes of Cu(II) adsorption and retention share some similarities but also differences with Zn(II) in the presence of sulfate. Similar to the behavior of Zn(II), increased Cu(II) adsorption and (more variably) retention occurs upon the introduction of sulfate (Fig. 3); however, since Cu–SO₄ complexes were negligible in our speciation models (Fig. 5), this increase is predominantly attributed to surface charge reduction by sulfate as a means of facilitating Cu ion adsorption/retention. In contrast with Zn(II), Cu(II) adsorption with increasing sulfate concentration remains relatively unchanged or in some cases declines, while Cu(II) retention with increasing sulfate only slightly increases, with more variability across all NP aggregate conditions. In addition to the comparably lower Cu(II) retention levels compared to Zn(II) retention, this suggests the presence of relatively weakly-bound Cu sorption complexes that can be more readily desorbed from the NP (aggregate) surfaces. Spectroscopic analyses corroborate this, with both bidentate edge- and corner-sharing sorption species removed under desorption conditions as evidenced by declines in their Cu–Fe coordination numbers, particularly under intermediate to high (0.06–0.18 M) sulfate conditions (–27% and –52% CN average decline, respectively, Table 3). This corresponds with a statistically reduced proportion of retained Cu(II) between the two endmembers of this concentration range (Fig. 3).

4.2. Effect of nanoparticle aggregation on Zn(II) and Cu(II) adsorption and retention

Our previous work described how the method and extent of FeOOH NP aggregation can impact the adsorption and retention of metal ions on FeOOH NPs (Dale et al., 2015; Gilbert et al., 2009; Stegemeier et al., 2015). For example, changes in pH or ionic strength produce more disordered, poorly crystalline aggregates, reducing surface area but also resulting in substantial interparticle pore space; these aggregates typically display lower initial metal ion adsorption levels but greater retention of metal ions in interparticle porous spaces compared to unaggregated NPs (Dale et al., 2015; Gilbert et al., 2009). The results of the Zn macroscopic experiments in the current study are generally

consistent with these findings, with pH- and ionic strength-induced aggregates displaying reduced Zn(II) adsorption but greater Zn(II) retention across all sulfate concentration levels relative to the control NPs, and with the higher pH/ionic strength aggregates retaining more Zn(II) than the lower pH/ionic strength aggregates (Fig. 1). Also consistent with earlier studies, Cu ion aggregation/retention is less systematically impacted by aggregation mechanism, likely indicating more consistent binding mechanism(s) across multiple aggregation states (Dale et al., 2015).

In contrast, increased temperature has been shown to produce more ordered, oriented FeOOH NPs with higher proportions of strong sorption sites and therefore, increased metal retention (Gilbert et al., 2009; Lee Penn et al., 2006; Stegemeier et al., 2015; Weidler et al., 1998; Yuwono et al., 2012). In the current study, the retention of Zn(II) and Cu(II) to FeOOH NP aggregates formed at 25 °C and 50 °C was consistently greater than that of the unaggregated control NPs, and in the case of Cu these aggregates retained the most of all NPs across the range of sulfate concentration examined (Figs. 1 and 3). However, the high-temperature (75 °C) aggregate displayed both lower adsorption and lower retention levels compared to the control NPs, likely through a significant growth in particle size and corresponding reduction in reactive surface area. Nanoparticles subjected to the same aging conditions from an earlier study (75 °C for 4 days) experienced a 6.2x increase in particle diameter (from 9.5 nm to 68 nm) and a 65% decrease in surface area (from 305 m²/g to 106 m²/g) (Stegemeier et al., 2015).

The retention of Zn(II) and Cu(II) averaged across the control and other NP aggregates as a function of sulfate concentration show that upon introducing sulfate, the average metal ion retention increased significantly and the variation in retention among the aggregates decreased, as evidenced by a continuous decrease in the standard error as sulfate concentration increases (Fig. 6). This suggests that the effect of sulfate is, on average, stronger than the effect of aggregation method on the retained metal fraction. A similar comparison was reported upon the introduction of and increase in chloride concentration in our prior study examining the effect of chloride concentration on Zn and Cu retention to FeOOH NPs (Chesne et al., 2014), which concluded that the presence of chloride had a greater impact than NP aggregation state on metal ion retention.

5. Conclusions

Macroscopic and spectroscopic investigations of metal ion adsorption/retention to FeOOH NPs and their aggregates provide important context to characterizing trace metal ion fate and transport in the environment, as well as assessing the role of FeOOH NPs as both a natural attenuation process and environmental remediation strategy.

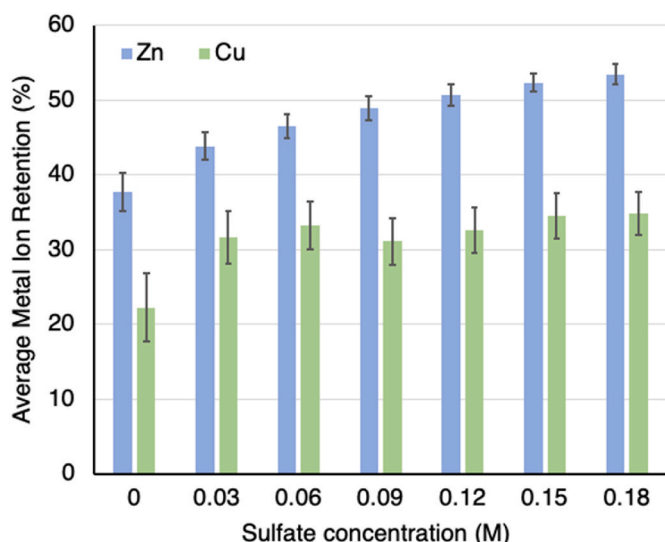


Fig. 6. Macroscopic metal retention averages across control and aggregated FeOOH nanoparticles as a function of sulfate concentration, with standard error bars representing the degree of variation among all forms of the nanoparticle substrate.

Results demonstrate that sulfate significantly and continuously enhances Zn(II) adsorption and retention to FeOOH NPs, with more subtle and variable increases in Cu(II) retention. We conclude that at sulfate concentrations consistent with that of seawater (0.03 M), the formation of ternary surface complexes and/or the reduction of electrostatic surface repulsion can facilitate enhanced metal ion uptake and retention. At higher sulfate concentrations consistent with acid mine drainage and brines (up to 0.3 M), surface charge neutralization further enhances metal ion retention through mechanisms including structural incorporation, although this process may be limited by the physical blocking of stronger adsorption sites by sulfate ions at the highest sulfate concentrations examined in this study. The distinct but complementary effects of chloride and sulfate, the two most common anions in seawater, on metal ion retention based on this and our prior studies (Chesne and Kim, 2014) indicate that the transport of metal-sorbed particles into increasingly saline conditions is unlikely to result in significant desorption of metals back into solution. Examining metal ion adsorption and desorption processes under even more complex saline environments will validate this assumption.

CRediT authorship contribution statement

Emma M. Kocik: Data curation, Formal analysis, Investigation, Methodology, Visualization, Writing – original draft, Writing – review & editing. **Abigail Kim:** Investigation, Methodology. **Miranda L. Aiken:** Writing – original draft, Writing – review & editing. **Lauren Smith:** Investigation, Methodology, Visualization, Writing – original draft. **Christopher S. Kim:** Conceptualization, Data curation, Formal analysis, Funding acquisition, Investigation, Methodology, Project administration, Resources, Supervision, Validation, Visualization, Writing – original draft, Writing – review & editing.

Declaration of competing interest

The authors declare the following financial interests/personal relationships which may be considered as potential competing interests: Christopher S. Kim reports financial support was provided by National Science Foundation. Christopher S. Kim reports financial support was provided by Research Corporation for Science Advancement. Emma Kocik reports financial support was provided by Arnold and Mabel Beckman Foundation. If there are other authors, they declare that they

have no known competing financial interests or personal relationships that could have appeared to influence the work reported in this paper.

Data availability

Data will be made available on request.

Acknowledgements

This work was funded by the National Science Foundation, Division of Earth Sciences, Grant #061821711, Cottrell College Science Award #6940/6912 from the Research Corporation, and the Arnold and Mabel Beckman Foundation through the Beckman Scholars Program. Use of the Stanford Synchrotron Radiation Lightsource, SLAC National Accelerator Laboratory, is supported by the U.S. Department of Energy, Office of Science, Office of Basic Energy Sciences under Contract No. DE-AC02-76SF00515. We also thank past members of the Kim Environmental Geochemistry Lab for their assistance with the macroscopic experiments.

References

- Alcacio, T.E., Hesterberg, D., Chou, J.W., Martin, J.D., Beauchemin, S., Sayers, D.E., 2001. Molecular scale characteristics of Cu(II) bonding in goethite-humate complexes. *Geochem. Cosmochim. Acta* 65 (9), 1355–1366. [https://doi.org/10.1016/S0016-7037\(01\)00546-4](https://doi.org/10.1016/S0016-7037(01)00546-4).
- Ali, M.A., Dzombak, D.A., 1996. Interactions of copper, organic acids, and sulfate in goethite suspensions. *Geochem. Cosmochim. Acta* 60 (24), 5045–5053.
- Auffan, M., Rose, J., Bottero, J.-Y., Lowry, G.V., Jolivet, J.-P., Wiesner, M.R., 2009. Towards a definition of inorganic nanoparticles from an environmental, health and safety perspective. *Nat. Nanotechnol.* 4 (10), 634–641.
- Balali-Mood, M., Naseri, K., Tahergorabi, Z., Khazdair, M.R., Sadeghi, M., 2021. Toxic mechanisms of five heavy metals: mercury, lead, chromium, cadmium, and arsenic. *Front. Pharmacol.* 12.
- Balistrieri, L., Murray, J., 1982. The adsorption of Cu, Pb, Zn, and Cd on goethite from major ion seawater. *Geochem. Cosmochim. Acta* 46 (7), 1253–1265.
- Banfield, J.F., Welch, S.A., Zhang, H., Ebert, T.T., Penn, R.L., 2000. Aggregation-based crystal growth and microstructure development in natural iron oxyhydroxide biomineralization products. *Science* 289 (5480), 751–754.
- Bethke, C.M., Farrell, B., Sharifi, M., 2023. The Geochemist's Workbench - Reactive Transport Modeling Guide. In: *Aqueous Solutions*, vol. 17. LLC.
- Blowes, D., Ptacek, C., Jambor, J., Weisener, C., 2005. *Environmental Geochemistry*.
- Bochatay, L., Persson, P., Lövgren, L., Brown Jr., G., 1997. XAFS study of Cu (II) at the water-goethite (α -FeOOH) interface. *J. Phys. Chem. B* 101 (22), 8212–8220.
- Brown Jr., G.E., Parks, G.A., 2001. Sorption of trace elements on mineral surfaces: modern perspectives from spectroscopic studies, and comments on sorption in the marine environment. *Int. Geol. Rev.* 43 (11), 963–1073.
- Chesne, R.B., Kim, C.S., 2014. Zn (II) and Cu (II) adsorption and retention onto iron oxyhydroxide nanoparticles: effects of particle aggregation and salinity. *Geochem. Trans.* 15 (1), 1–12.
- Collins, C.R., Ragnarsdottir, K.V., Sherman, D.M., 1999. Effect of inorganic and organic ligands on the mechanism of cadmium sorption to goethite. *Geochem. Cosmochim. Acta* 63 (19–20), 2989–3002.
- Dale, J., Stegemeier, J., Kim, C., 2015. Aggregation of nanoscale iron oxyhydroxides and corresponding effects on metal uptake, retention, and speciation: I. Ionic-strength and pH. *Geochem. Cosmochim. Acta* 148, 100–112.
- Dzombak, D.A., Morel, F.M., 1991. *Surface Complexation Modeling: Hydrated Ferric Oxide*. John Wiley & Sons.
- Elzinga, E., Peak, D., Sparks, D., 2001. Spectroscopic studies of Pb (II)-sulfate interactions at the goethite-water interface. *Geochem. Cosmochim. Acta* 65 (14), 2219–2230.
- EPA, U.S., 2003. *Drinking Water Advisory: Consumer Acceptability Advice and Health Effects Analysis on Sulfate*, p. 2.
- García-Sánchez, A., Alastuey, A., Querol, X., 1999. Heavy metal adsorption by different minerals: application to the remediation of polluted soils. *Sci. Total Environ.* 242 (1–3), 179–188.
- Gilbert, B., Lu, G., Kim, C.S., 2007. Stable cluster formation in aqueous suspensions of iron oxyhydroxide nanoparticles. *J. Colloid Interface Sci.* 313 (1), 152–159.
- Gilbert, B., Ono, R.K., Ching, K.A., Kim, C.S., 2009. The effects of nanoparticle aggregation processes on aggregate structure and metal uptake. *J. Colloid Interface Sci.* 339 (2), 285–295.
- Guo, H., Barnard, A.S., 2013. Naturally occurring iron oxide nanoparticles: morphology, surface chemistry and environmental stability. *J. Mater. Chem. A* 1 (1), 27–42. <https://doi.org/10.1039/C2TA00523A>.
- Guyodo, Y., Mostrom, A., Lee Penn, R., Banerjee, S.K., 2003. From nanodots to nanorods: oriented aggregation and magnetic evolution of nanocrystalline goethite. *Geophys. Res. Lett.* 30 (10).
- Hochella, M.F., 1990. Atomic structure, microtopography, composition, and reactivity of mineral surfaces. *Rev. Mineral. Geochem.* 23 (1), 87–132.

- Hoins, U., Charlet, L., Sticher, H., 1993. Ligand effect on the adsorption of heavy metals: the sulfate — cadmium — goethite case. *Water Air Soil Pollut.* 68 (1), 241–255. <https://doi.org/10.1007/BF00479406>.
- Hou, T., Xu, R., Tiwari, D., Zhao, A., 2007. Interaction between electrical double layers of soil colloids and Fe/Al oxides in suspensions. *J. Colloid Interface Sci.* 310 (2), 670–674.
- Juang, R.-S., Wu, W.-L., 2002. Adsorption of sulfate and copper(II) on goethite in relation to the changes of zeta potentials. *J. Colloid Interface Sci.* 249 (1), 22–29. <https://doi.org/10.1006/jcis.2002.8240>.
- Juillot, F., Maréchal, C., Ponthieu, M., Cacaly, S., Morin, G., Benedetti, M., Hazemann, J., Proux, O., Guyot, F., 2008. Zn isotopic fractionation caused by sorption on goethite and 2-Lines ferrihydrite. *Geochem. Cosmochim. Acta* 72 (19), 4886–4900.
- Kim, C., Lentini, C., Waychunas, G., 2008. Synchrotron-based studies of metal adsorption and structural incorporation with iron oxyhydroxide nanoparticles. *Adsorption of Metals by Geomedia II: Variables, Mechanisms, and Model Applications* 478.
- Kim, C.S., Rytuba, J.J., Brown, G.E., 2004. EXAFS study of mercury(II) sorption to Fe- and Al-(hydr)oxides. II. Effects of chloride and sulfate. *J. Colloid Interface Sci.* 270 (1), 9–20. <https://doi.org/10.1016/j.jcis.2003.07.029>.
- Lee Penn, R., Erbs, J.J., Gulliver, D.M., 2006. Controlled growth of alpha-FeOOH nanorods by exploiting-oriented aggregation. *J. Cryst. Growth* 293 (1), 1–4. <https://doi.org/10.1016/j.jcrysgro.2006.05.005>.
- Lee, S., Anderson, P.R., 2005. EXAFS study of Zn sorption mechanisms on hydrous ferric oxide over extended reaction time. *J. Colloid Interface Sci.* 286 (1), 82–89.
- Li, S.-z., Xu, R.-k., 2008. Electrical double layers' interaction between oppositely charged particles as related to surface charge density and ionic strength. *Colloids Surf. A Physicochem. Eng. Asp.* 326 (3), 157–161.
- Liu, J., Zhu, R., Liang, X., Ma, L., Lin, X., Zhu, J., He, H., Parker, S.C., Molinari, M., 2018. Synergistic adsorption of Cd (II) with sulfate/phosphate on ferrihydrite: an in situ ATR-FTIR/2D-COS study. *Chem. Geol.* 477, 12–21.
- Lowry, G.V., Shaw, S., Kim, C.S., Rytuba, J.J., Brown, G.E., 2004. Macroscopic and microscopic observations of particle-facilitated mercury transport from New Idria and Sulphur Bank mercury mine tailings. *Environ. Sci. Technol.* 38 (19), 5101–5111.
- Luo, C., Routh, J., Dario, M., Sarkar, S., Wei, L., Luo, D., Liu, Y., 2020. Distribution and mobilization of heavy metals at an acid mine drainage affected region in South China, a post-remediation study. *Sci. Total Environ.* 724, 138122.
- Nachtegaal, M., Sparks, D.L., 2004. Effect of iron oxide coatings on zinc sorption mechanisms at the clay-mineral/water interface. *J. Colloid Interface Sci.* 276 (1), 13–23.
- Nordstrom, D.K., Alpers, C.N., 1999. Negative pH, efflorescent mineralogy, and consequences for environmental restoration at the Iron Mountain Superfund site, California. *Proc. Natl. Acad. Sci. USA* 96 (7), 3455–3462.
- Ostergren, J.D., Brown Jr., G.E., Parks, G.A., Persson, P., 2000. Inorganic ligand effects on Pb (II) sorption to goethite (α -FeOOH): II. Sulfate. *J. Colloid Interface Sci.* 225 (2), 483–493.
- Parkman, R., Charnock, J., Bryan, N., Livens, F., Vaughan, D., 1999. Reactions of copper and cadmium ions in aqueous solution with goethite, lepidocrocite, mackinawite, and pyrite. *Am. Mineral.* 84 (3), 407–419.
- Peacock, C.L., Sherman, D.M., 2004. Copper (II) sorption onto goethite, hematite and lepidocrocite: a surface complexation model based on ab initio molecular geometries and EXAFS spectroscopy. *Geochem. Cosmochim. Acta* 68 (12), 2623–2637.
- Ponthieu, M., Juillot, F., Hiemstra, T., Van Riemsdijk, W., Benedetti, M., 2006. Metal ion binding to iron oxides. *Geochem. Cosmochim. Acta* 70 (11), 2679–2698.
- Rytuba, J.J., 2000. Mercury mine drainage and processes that control its environmental impact. *Sci. Total Environ.* 260 (1–3), 57–71.
- Shi, M., Min, X., Ke, Y., Lin, Z., Yang, Z., Wang, S., Peng, N., Yan, X., Luo, S., Wu, J., Wei, Y., 2021. Recent progress in understanding the mechanism of heavy metals retention by iron (oxyhydr)oxides. *Sci. Total Environ.* 752, 141930 <https://doi.org/10.1016/j.scitotenv.2020.141930>.
- Singh, D., McLaren, R.G., Cameron, K.C., 2008. Effect of pH on zinc sorption–desorption by soils. *Commun. Soil Sci. Plant Anal.* 39 (19–20), 2971–2984.
- Stegemeier, J., Reinsch, B., Lentini, C., Dale, J., Kim, C., 2015. Aggregation of nanoscale iron oxyhydroxides and corresponding effects on metal uptake, retention, and speciation: II. Temperature and time. *Geochem. Cosmochim. Acta* 148, 113–129.
- Stumm, W., Morgan, J.J., 2012. *Aquatic Chemistry: Chemical Equilibria and Rates in Natural Waters*. John Wiley & Sons.
- Swedlund, P.J., Webster, J.G., Miskelly, G.M., 2009. Goethite adsorption of Cu(II), Pb(II), Cd(II), and Zn(II) in the presence of sulfate: properties of the ternary complex. *Geochem. Cosmochim. Acta* 73 (6), 1548–1562. <https://doi.org/10.1016/j.gca.2008.12.007>.
- Trivedi, P., Axe, L., Tyson, T.A., 2001. An analysis of zinc sorption to amorphous versus crystalline iron oxides using XAS. *J. Colloid Interface Sci.* 244 (2), 230–238.
- Van Der Merwe, D., Carpenter, J.W., Nietfeld, J.C., Miesner, J.F., 2011. Adverse health effects in Canada geese (*Branta canadensis*) associated with waste from zinc and lead mines in the Tri-State Mining District (Kansas, Oklahoma, and Missouri, USA). *J. Wildl. Dis.* 47 (3), 650–660.
- Waychunas, G., Fuller, C., Davis, J., 2002. Surface complexation and precipitate geometry for aqueous Zn (II) sorption on ferrihydrite I: X-ray absorption extended fine structure spectroscopy analysis. *Geochem. Cosmochim. Acta* 66 (7), 1119–1137.
- Webb, S.M., 2005. SIXpack: a graphical user interface for XAS analysis using IFEFFIT. *Phys. Scripta* 2005 (T115), 1011. <https://doi.org/10.1238/Physica.Topical.115a01011>.
- Webster, J.G., Swedlund, P.J., Webster, K.S., 1998. Trace metal adsorption onto an acid mine drainage iron (III) oxy hydroxy sulfate. *Environ. Sci. Technol.* 32 (10), 1361–1368.
- Weesner, F.J., Bleam, W.F., 1998. Binding characteristics of Pb²⁺ on anion-modified and pristine hydrous oxide surfaces studied by electrophoretic mobility and X-ray absorption spectroscopy. *J. Colloid Interface Sci.* 205 (2), 380–389.
- Weidler, P.G., Hug, S.J., Wetche, T.P., Hiemstra, T., 1998. Determination of growth rates of (100) and (110) faces of synthetic goethite by scanning force microscopy. *Geochem. Cosmochim. Acta* 62 (21), 3407–3412. [https://doi.org/10.1016/S0016-7037\(98\)00251-8](https://doi.org/10.1016/S0016-7037(98)00251-8).
- Yuwono, V.M., Burrows, N.D., Soltis, J.A., Do, T.A., Penn, R.L., 2012. Aggregation of ferrihydrite nanoparticles in aqueous systems. *Faraday Discuss* 159 (1), 235–245.
- Zhang, G., Peak, D., 2007. Studies of Cd (II)-sulfate interactions at the goethite–water interface by ATR-FTIR spectroscopy. *Geochem. Cosmochim. Acta* 71 (9), 2158–2169.